Onsite magnetic moment through cation distribution and magnetocrystalline anisotropy studies in $NiFe_{2-x}R_xO_4$ (R = Y and Lu; x = 0, 0.05, and 0.075)

Ugendar Kodam, Kamala Bharathi K, Raghavendra Reddy V, Sudhindra Rayaprol, Vasudeva Siruguri, and Markandeyulu Garimalle

Citation: J. Appl. Phys. **121**, 055101 (2017); doi: 10.1063/1.4973880
View online: http://dx.doi.org/10.1063/1.4973880
View Table of Contents: http://aip.scitation.org/toc/jap/121/5
Published by the American Institute of Physics

Onsite magnetic moment through cation distribution and magnetocrystalline anisotropy studies in $NiFe_{2-x}R_xO_4$ (R = Y and Lu; $x = 0$, 0.05, and 0.075)

Ugendar Kodam,[1] Kamala Bharathi K,[2] Raghavendra Reddy V,[3] Sudhindra Rayaprol,[4] Vasudeva Siruguri,[4] and Markandeyulu Garimalle[1,a)]

[1]*Advanced Magnetic Materials Laboratory, Department of Physics, Indian Institute of Technology Madras, Chennai 600 036, India*
[2]*SRM University, Department of Physics and Nanotechnology, Research Institute, Kattankulathur, Chennai 603203, India*
[3]*UGC-DAE Consortium for Scientific Research, University Campus, Khandwa Road, Indore 452 001, India*
[4]*UGC-DAE Consortium for Scientific Research, Mumbai center, Bhabha Atomic Research Centre, Trombay, Mumbai 400 085, India*

(Received 23 August 2016; accepted 28 December 2016; published online 1 February 2017)

Onsite magnetic moments through cation distribution and magnetocrystalline anisotropy studies of $NiFe_{2-x}R_xO_4$ (R = Y and Lu; $x = 0$, 0.05, and 0.075) compounds were investigated, and the results are discussed and presented in this paper. All the compounds were prepared by solid state reaction, and the compounds formed in the cubic inverse spinel phase with the space group $Fd\bar{3}m$. The cation distribution, bond lengths, u-parameter, *etc*. were estimated through the Rietveld refinement of XRD patterns. Increment in the lattice constant was observed upon partial substitution of Fe^{3+} by Y^{3+}/Lu^{3+}. The presence of all elements and their ionic states were confirmed from X-ray photoelectron spectroscopy studies. Analyses of Mössbauer spectra revealed that the hyperfine fields and the magnetic moments at the B-site (and hence net moment) decreased with increasing Y^{3+}/Lu^{3+} occupancy and that the compounds exhibited a Néel-type, collinear ferrimagnetic structure. Magnetization measurements revealed that the magnetic moment decreased with Y^{3+}/Lu^{3+} substitution. The high field regimes of the magnetization curves were modeled using the law of approach to the saturation magnetization equation, and the first order cubic anisotropy constants (K_1) were calculated. The temperature variation of K_1 and effects of Y^{3+}/Lu^{3+} substitution are explained. *Published by AIP Publishing*. [http://dx.doi.org/10.1063/1.4973880]

I. INTRODUCTION

Nickel ferrite - $NiFe_2O_4$, one of the most important spinel ferrites, has potential applications in spin-filters,[1,2] spintronics,[3] magnetic recording media,[4] multiferroics,[5] *etc*.[6,7] Determination of the distribution of cations among tetrahedral (A) sites and the octahedral (B) sites in $NiFe_2O_4$ and its derivatives is of considerable interest as the understanding of the magnetic properties of these spinel ferrites depends on the sites occupied by the cations.[8,9] Magnetic anisotropy is known to play a vital role in magnetic recording media[10] whose properties depend on magnetostriction, particle size, shape, orientation, *etc*.[4,6,7] Temperature dependent magnetic anisotropy studies therefore are useful towards applications such as heat assisted magnetic recording.[11]

Partial substitutions of non-magnetic 3*d*-transition metal ions and ions of lower atomic number in $NiFe_2O_4$ have been reported to affect the cation distribution and hence its magnetic, electric, and dielectric properties.[12–15] The triangular Yafet-Kittel structure in $NiFe_{0.3}Cr_{1.7}O_4$, due to the alteration of the collinear Néel type ferrimagnetic structure of $NiFe_2O_4$ has been reported.[12] Heiba *et al*.[13] through Mössbauer spectra and refinement of x-ray diffraction (XRD) patterns have shown that in $NiFe_{2-x}Ga_xO_4$ ($x = 0$, 0.2, 0.4, 0.6, 0.8, and 1), Ni^{2+} ions were distributed between A and B sites for all x, whereas Ga^{3+} occupied mainly the A sites for $x < 0.6$ and the B sites for $x \geq 0.6$. Through Mössbauer spectra, the occupation of Cr^{3+} and Al^{3+} for Fe^{3+} at the octahedral sites and a corresponding decrease in saturation magnetization of Ni-Zn ferrite have been reported by Ghasemin and Mousavinia.[14]

Substitution of Gd^{3+} (having spin only magnetic moment) for Fe^{3+} has resulted in the increased coercive field, decreased magnetization, magnetostriction, and magnetocrystalline anisotropy.[16–18] On the other hand, the partial substitution rare-earth ion having spin-orbit interactions has led to the structural distortion and development of magnetocapacitance and magnetoelectric effect.[16,19–21] Induced trigonal distortion and decrease in longitudinal magnetostriction and magnetocrystalline anisotropy upon substitution of Nd^{3+} for Fe^{3+} in $CoFe_2O_4$ have been reported.[20] Substitution of part of Fe^{3+} by Nd^{3+}, Sm^{3+}, Ho^{3+}, and Dy^{3+} has led to deviation from centrosymmetry, causing the development of ferroelectricity, magnetoelectric effect, and affected magnetic and electrical properties.[16,21,22] In $NiFe_{2-x}Yb_xO_4$ ($x = 0$, 0.05, and 0.075), the replacement of Fe^{3+} ions by Yb^{3+} ions has been reported to lead to a decrease in the B-site magnetic moment and hyperfine interaction parameters.[23] A decrease in magnetization and Curie temperature upon partial substitution of Fe^{3+} by R^{3+} (R = Ce, Sm, Gd, Tb, Dy, Ho, Er, and Yb) in $NiFe_2O_4$ has been reported.[6,7,16,19,21–23] This has been attributed to the reduction in the number of Fe^{3+}-O-Fe^{3+} bonds and weak

a)Electronic mail: mark@iitm.ac.in

R-Fe exchange coupling that replaced the strong itinerant Fe-Fe exchange coupling. The substitution of non-magnetic rare-earth ions has been reported to alter the cation distribution considerably and largely influence the intrinsic coercive field and saturation magnetization values.[15,18,24,25] A large decrease in the coercive field and saturation magnetization has been reported.[24,25] Şoka *et al.*[15,18] have reported a decrease in remnant and saturation magnetic flux densities of $Ni_{0.42}Zn_{0.58}Fe_2O_4$ upon substitution of Fe^{3+} ions by R^{3+} (R = La and Y).

In this paper, the effect of partial substitution of Fe^{3+} by non-magnetic Y^{3+} and Lu^{3+} cations (ionic radius of Y^{3+} is 0.89 Å, Lu^{3+} is 0.85 Å, and Fe^{3+} is 0.63 Å) on cation distribution and on-site magnetic moments is presented.

II. EXPERIMENTAL DETAILS

Polycrystalline $NiFe_{2-x}R_xO_4$ compounds (R = Y and Lu; $x = 0$, 0.05, and 0.075) were prepared starting from NiO (99.96% pure), Fe_2O_3, Y_2O_3, and Lu_2O_3 (99.99% pure) by the solid state reaction method. The powders of the starting materials were taken in stoichiometric ratios and were ground using an agate mortar and pestle for 3 h, and the mixtures were heat treated in air at 1200 °C for 12 h. The formation of the phases was confirmed by taking powder x-ray diffraction (XRD) patterns using a PANalytical (X'pert PRO) x-ray diffractometer employing Cu K_α radiation. X-ray photoelectron spectra (XPS) in Fe 2*p*, Ni 2*p*, Y 3*d*, and O 1*s* regions were recorded employing a microfocused monochromatic X-ray source having an energy resolution of 0.47 eV at FWHM, using a Sigma Probe-Surface Analysis instrument. The binding energies (BE) of all the spectra were charge corrected with reference to the C 1*s* value at 284 eV. The pressure in the chamber during the experiments was maintained at 4.5×10^{-10} Torr. Raman active vibrational modes were recorded using a Horiba Jobin Yvon HR800 UV: Raman Division, Raman spectrometer, with an excitation wavelength of 633 nm, in the wavenumber range of 180–800 cm^{-1}.

Magnetization was measured using an MPMS SQUID based vibrating sample magnetometer (VSM). Neutron diffraction measurements were carried out using a powder diffractometer-II (wavelength, 1.249 Å), at the Dhruva reactor, BARC (Bhabha Atomic Research Centre), Mumbai. ^{57}Fe Mössbauer measurements were carried out in transmission mode at 5 K.

III. RESULTS AND DISCUSSION

A. Structural details

The x-ray diffraction (XRD) patterns of $NiFe_{2-x}R_xO_4$ (R = Y and Lu; $x = 0$, 0.05, and 0.075) are shown in Fig. 1. All the compounds crystallized in the cubic inverse spinel structure (space group, $Fd\bar{3}m$) with small amounts of $RFeO_3$ (R = Y and Lu) as secondary phases in the $x = 0.05$ and 0.075 compounds. The values of weight fractions of the inverse spinel phase and $YFeO_3$ phase, respectively, are 0.98 and 0.02 in $NiFe_{1.95}Y_{0.05}O_4$ and 0.95 and 0.05 in $NiFe_{1.925}Y_{0.075}O_4$. For those of $LuFeO_3$, they are 0.96 and 0.04 in $NiFe_{1.95}Lu_{0.05}O_4$ and 0.93 and 0.07 in $NiFe_{1.925}Lu_{0.075}O_4$.

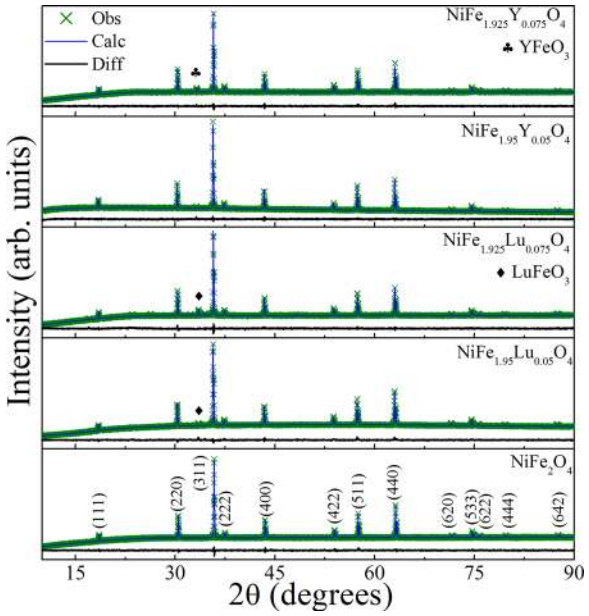

FIG. 1. Rietveld refined XRD patterns of $NiFe_{2-x}R_xO_4$ (R = Y and Lu; $x = 0$, 0.05, and 0.075).

The Rietveld refinement of the XRD patterns was carried out using General Sturucture Analysis System (GSAS) software with EXPUGI interface. The refinement parameters, *viz.*, ω_{rp} (weighted refined parameter), χ^2 (goodness of the fit), lattice constant values, bond lengths, and bond angles, are given in Table I. The observed increase in the lattice constant (compared with $NiFe_2O_4$) is due to the replacement of the Fe^{3+} ions (0.63 Å) by Y^{3+} (0.89 Å) and Lu^{3+} (0.85 Å) ions. In addition, the O^{2-}-Fe^{3+}(B) bond length is seen to increase and the O^{2-}-Fe^{3+}(A) bond length is seen to decrease. This confirms that the Y^{3+} and Lu^{3+} ions substituted for Fe^{3+} ions occupy the octahedral site.

It is known that in $NiFe_2O_4$, all the tetrahedral sites are occupied by Fe^{3+} ions, 50% of octahedral sites are occupied by Ni^{2+} ions, and the rest are occupied by the remaining Fe^{3+} ions.[6,7] Thus, in the compounds investigated, the partial replacement of Fe^{3+} ions by Y^{3+} or Lu^{3+} changes the cationic distribution between the tetrahedral (A) sites and octahedral (B) sites. The decrease in the occupancy of Fe^{3+} ions at the B-site for compounds containing Y^{3+} and Lu^{3+} confirms that Y^{3+} and Lu^{3+} favour the B-site. The inversion parameter is found to be 0.99 for $NiFe_2O_4$, 0.98 and 0.99 for $NiFe_{2-x}Y_xO_4$ for $x = 0.05$ and 0.075, respectively, and 0.94 and 0.93 for $NiFe_{2-x}Lu_xO_4$ for $x = 0.05$ and 0.075, respectively.

The ideal value of the oxygen parameter (*u*-parameter, say, u_0) quantifying the degree of distortion of the anion sublattice is equal to 0.375.[6,7] For this ideal value, O^{2-} ions form a cubic closed packed configuration. This ideal pattern is slightly deformed in the real lattice, and the *u*-parameters are slightly higher (in the range of 0.38–0.39) than u_0.[26,27] The values of *u*-parameters for the Y^{3+} and Lu^{3+} substituted compounds were calculated, using the values of lattice constants, the radius of oxygen ion ($R_o = 1.382$ Å), and r_A - the radius of the cation (Fe^{3+}) occupying the A-site (0.63 Å), from the relation[6,7]

TABLE I. Structural parameters of $NiFe_{2-x}R_xO_4$ (R = Y and Lu; $x = 0$, 0.05, and 0.075).

Compound		$NiFe_2O_4$	$NiFe_{2-x}Y_xO_4$		$NiFe_{2-x}Lu_xO_4$	
Composition (values of ***x***)		0	0.05	0.075	0.05	0.075
X^2		1.005	1.15	1.11	1.25	1.68
ω_{rp} (%)		1.55	1.70	1.55	1.44	2.08
Lattice constant (Å)		8.3393(6)	8.3411(6)	8.3406(4)	8.3479(8)	8.3520(9)
Bond length (Å)	O^{2-}-Fe^{3+} (B)	2.031	2.034	2.080	2.055	2.072
	O^{2-}-Fe^{3+} (A)	1.902	1.897	1.815	1.863	1.836
Bond angle (deg)	Fe^{3+}(A)-O^{2-}-Fe^{3+}/R^{3+}(B)	124.06	123.16	125.06	124.00	124.63
	Ni^{2+}-O^{2-}-Ni^{2+}	91.68	93.01	90.29	91.77	90.9
	O^{2-}-Fe^{3+} (A)-O^{2-}	109.47	109.47	109.47	109.47	109.47
	O^{2-}-Fe^{3+} (B)-O^{2-}	93.08	93.01	90.29	91.80	90.90
Occupancies	Ni_B^{2+}	0.498	0.497	0.496	0.473	0.465
	Fe_B^{3+}	0.498	0.460	0.458	0.449	0.430
	R_B^{3+}	-	0.025	0.038	0.023	0.035
	Fe_A^{3+}	1.000	0.998	0.999	1.002	0.994
Inversion parameter		0.99	0.98	0.99	0.94	0.93
u-parameter		0.389(3)	0.389(2)	0.389(3)	0.389(1)	0.389(1)

$$r_A = \left(u - \frac{1}{4}\right)a\sqrt{3} - R_o. \quad (1)$$

The obtained values of *u*-parameters are given in Table I. For all the $NiFe_{2-x}R_xO_4$ compounds ($x = 0$, 0.05, and 0.075; R = Y and Lu) investigated, $u > u_{ideal}$ (i.e., $u > u_0$), which means that the O^{2-} ions move away from the cations in the tetrahedral A-site along the ⟨111⟩ direction.

The back scattered electron (BSE) images shown in Fig. 2 clearly indicate two distinct contrasts (except in $NiFe_2O_4$) that correspond to their respective primary inverse spinel phase and the secondary $RFeO_3$ phase. The spot mode (in the regions of the $RFeO_3$ phase) energy dispersive x-ray (EDX) spectra of $NiFe_{2-x}R_xO_4$ (R = Y and Lu; $x = 0$ and 0.075) compounds, shown in Fig. 2, indicate pronounced peaks for all the elements present in the materials.

B. X-ray photoelectron spectroscopic (XPS) studies

The XPS spectra of Fe 2*p* in $NiFe_{1.925}R_{0.075}O_4$ (R = Y and Lu) are shown in Figs. 3(a) and 4(a). The Fe 2*p* spectrum consists of two spin-orbit-split peaks, *viz.*, $2p_{3/2}$ and $2p_{1/2}$. After deconvoluting the Fe $2p_{3/2}$ peak, the concentrations of Fe^{3+} and Fe^{2+} ions are obtained as 92% and 8%, respectively, in $NiFe_{1.925}Y_{0.075}O_4$. For the $NiFe_{1.925}Lu_{0.075}O_4$ compound, the concentrations of Fe^{3+} and Fe^{2+} ions are obtained as 61.6% and 38.4%, respectively. Figs. 3(b) and 4(b) show the XPS spectra of Ni 2*p*. Two peaks at 855 eV and 872.4 eV in $NiFe_{1.925}Y_{0.075}O_4$ and 853.7 eV and 871.4 eV in $NiFe_{1.925}Lu_{0.075}O_4$, respectively, correspond to $2p_{3/2}$ and $2p_{1/2}$. These binding energies (BE) correspond to a valency of +2 of the Ni ion. Kim *et al.*[28] have reported the presence of Ni^{2+} in $Ni_{0.96}Fe_{2.04}O_4$.

The XPS spectra of Y 3*d* is shown in Fig. 3(c). The two peaks at 158.8 eV and 156.5 eV are assigned to spin-orbit-split $3d_{5/2}$ and $3d_{3/2}$, respectively. The $3d_{5/2}$ peak at 158.8 eV is an indicator of the +3 oxidation state of Y.[29] Chambers *et al.*[29] have observed the Y $3d_{5/2}$ peak at 158.3 eV and the Y $3d_{3/2}$ peak at 160.3 eV in Y thin films sputtered on Si(100). The XPS spectrum of Lu 4*d* is shown in Fig. 4(c). The two spin-orbit-split $4d_{5/2}$ and $4d_{3/2}$ peaks are seen at 195.8 eV and 205.7 eV, respectively. The $4d_{5/2}$ peak at 195.8 eV is an indicator of the +3 oxidation state of Lu.[30] Figs. 3(d) and 4(d) show the O 1*s* spectra. The peaks at 527.2 eV in Fig. 3(d) and at 528.4 eV in Fig. 4(d) are ascribed to O^{2-} ions at the vertices of octahedra, whereas the peaks at 530.9 eV in Fig. 3(d)) and at 530 eV in Fig. 4(d) are ascribed to those at the vertices of tetrahedra.[28]

C. Raman spectroscopic studies

In order to confirm the presence (or absence) of other phases such as FeO, α-Fe_2O_3, and NiO, the compounds were further investigated using Raman spectra. Fig. 5 shows the room temperature Raman spectra of $NiFe_{2-x}R_xO_4$ (R = Y and Lu; $x = 0$, 0.05, and 0.075) compounds. The peaks were fitted to the Lorentzian function. Five Raman modes, *viz.*, A_{1g} (1) + E_g (1) + T_{2g} (3), corresponding to the inverse spinel phase (with the space group O_h^7)[31,32] were identified and are indicated in Fig. 5. Additional peaks observed in all the compounds are attributed to the presence of short-range ordering of Ni^{2+} and Fe^{3+} ions at the B-site.[32,33] No Raman mode corresponding to the $RFeO_3$ (R = Y and Lu) phase or other phases is observed.

An indication for the substitution of Y^{3+} or Lu^{3+} for Fe^{3+} at the B-site could be the T_{2g}(3) Raman mode,[33] which is associated with the FeO_6 octahedron in the region 560–590 cm^{-1}. In addition, this mode indicates the degree of B-site ordering.[33] Table II lists the positions of T_{2g}(3) Raman mode in all the compounds investigated. The wavenumber of T_{2g}(3) mode decreases for Lu^{3+} substituted compounds, whereas it increases for the Y^{3+} substituted compounds. In an ideal situation, the wavenumber of T_{2g}(3) mode should decrease for the Y^{3+} or Lu^{3+} substituted compounds. This is because of the fact that the force constant *k*

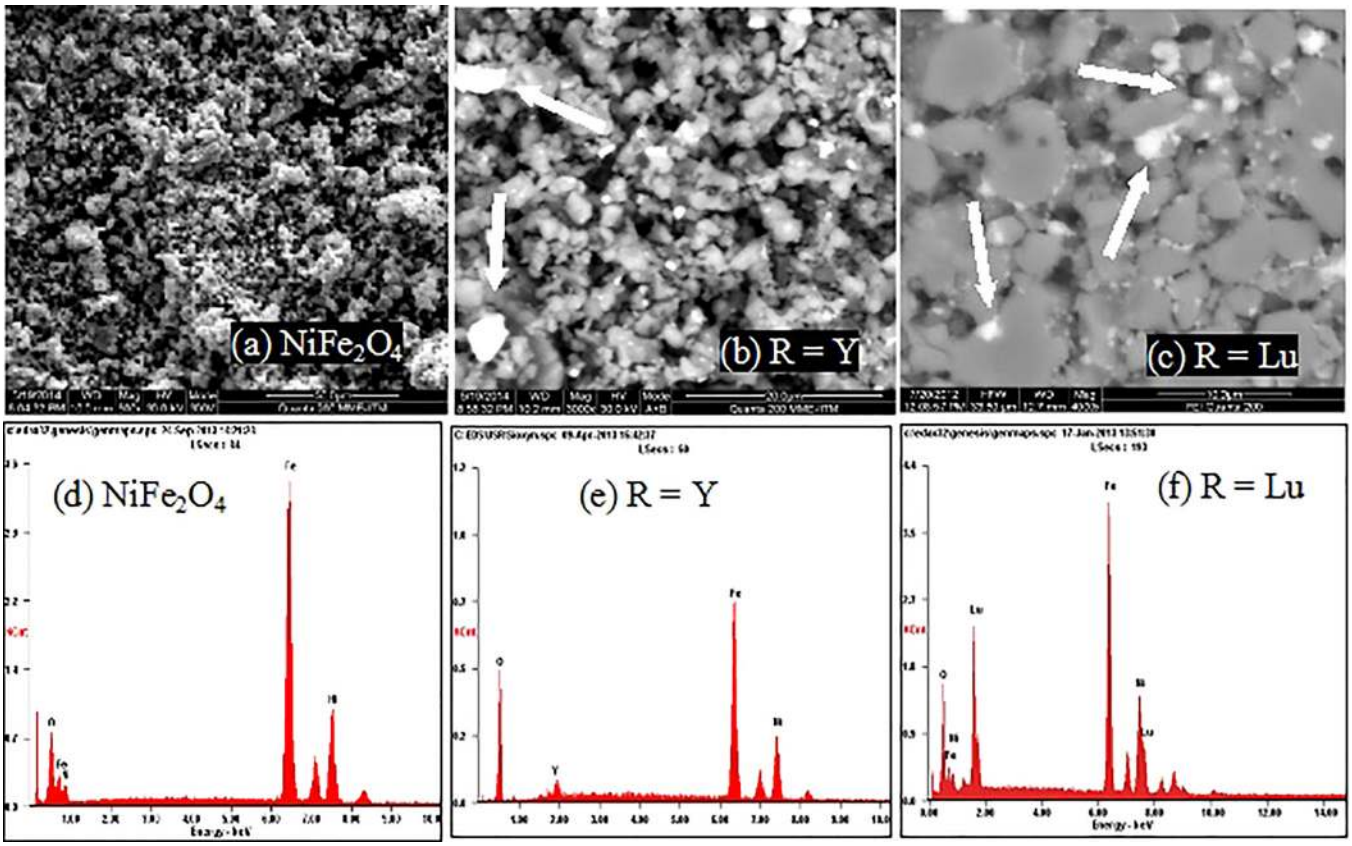

FIG. 2. BSE images ((a)–(c)) and EDX spectra ((d)–(f)) elemental mapping of $NiFe_{2-x}R_xO_4$ ($x = 0$ and 0.075; R = Y and Lu) compounds. The $RFeO_3$ phase is marked with arrows.

(which is directly depends on the product of charge available at B-site cations and oxygen anions; inversely proportional to the cube of the octahedral bond length) decreases and the effective mass of atoms μ increases for the Y^{3+} or Lu^{3+} substituted compounds.

D. Magnetization studies

Magnetization was measured at 20 K, 50 K, 100 K, 150 K, 200 K, 250 K, and 300 K, and the magnetization curves of $NiFe_{2-x}R_xO_4$ (R = Y and Lu; $x = 0$, 0.05, and 0.075) are shown in Fig. 6. The value of M_s (20 K) of

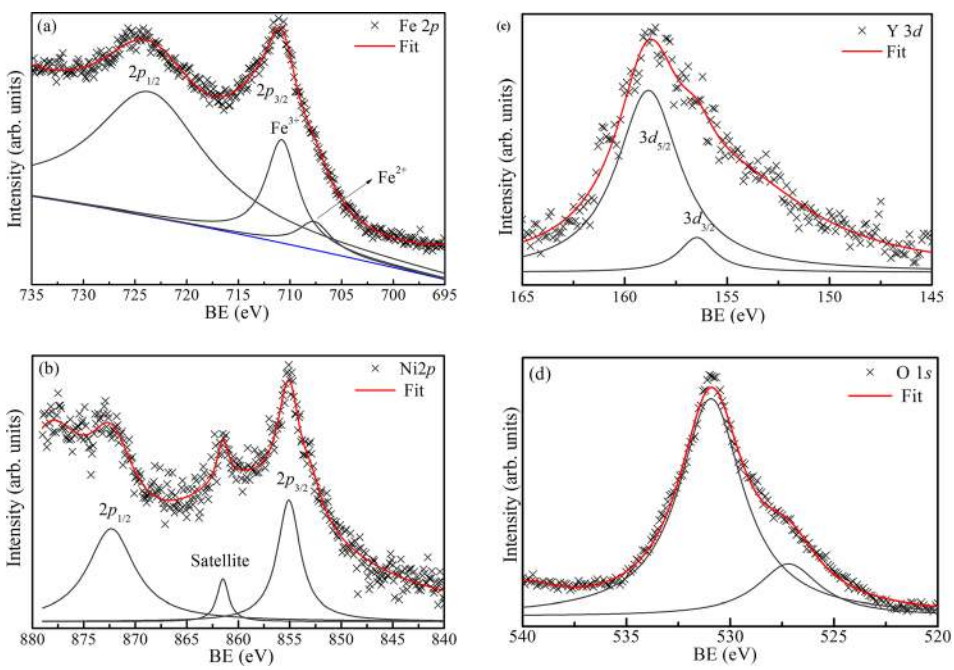

FIG. 3. XPS spectra of Fe 2*p* (a), Ni 2*p* (b), Y 3*d* (c), and O 1*s* (d) in $NiFe_{1.925}Y_{0.075}O_4$.

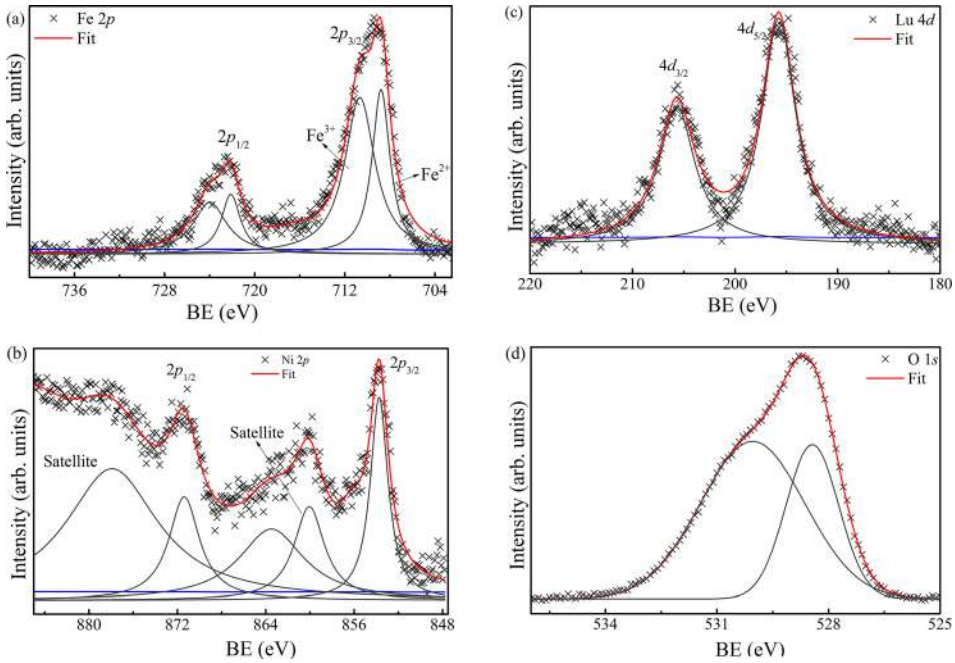

FIG. 4. XPS spectra of Fe 2*p* (a), Ni 2*p* (b), Lu 4*d* (c), and O 1*s* (d) in $NiFe_{1.925}Lu_{0.075}O_4$.

$NiFe_2O_4$ is 2.36 μ_B/f.u., in agreement with the reported value of 2.3 μ_B/f.u.[7] The values of M_s (20 K) of $NiFe_{2-x}Y_xO_4$ are 2.34 μ_B/f.u. and 1.87 μ_B/f.u. and in $NiFe_{2-x}Lu_xO_4$ are 2.29 μ_B/f.u. and 2.22 μ_B/f.u. for $x = 0.05$ and 0.075, respectively. The moment of $NiFe_2O_4$ calculated using Hund's rules is 2.3 μ_B/f.u. and substituted (moments of Y^{3+} and Lu^{3+} are zero) $NiFe_2O_4$ are 2.05 μ_B/f.u. and 1.925 μ_B/f.u. for $x = 0.05$ and 0.075, respectively. These values are in fair agreement with the experimentally determined magnetization. $RFeO_3$ (R = Y and Lu) compounds are antiferromagnetic with magnetization <1 emu/g.[34,35] In addition, the $RFeO_3$ phase fraction was found to be ≤7% in the present investigations. The contribution of $RFeO_3$ to the magnetization is thus 0.07 emu/g, which can be neglected.

The inversion parameter (λ) and site magnetic moments from magnetization were calculated using the equations

$$m_A = (1-\lambda)m_{Ni^{2+}} + \lambda m_{Fe^{3+}}, \tag{2}$$

$$m_B = \lambda m_{Ni^{2+}} + (2-\lambda-x)m_{Fe^{3+}} + x\lambda m_{R^{3+}}, \tag{3}$$

where m_A and m_B are the magnetic moments of the A-site and B-site, respectively. λ was calculated using the reported moments of Ni^{2+} and Fe^{3+} (2.3 μ_B and 5 μ_B, respectively).[7] The values of λ are 0.98 for $NiFe_2O_4$, 0.94 and 0.99 for $NiFe_{2-x}Y_xO_4$, and 0.95 and 0.94 for $NiFe_{2-x}Lu_xO_4$ for $x = 0.05$ and 0.075, respectively, which are in agreement with those obtained from the refinements of XRD patterns.

The M-H data at fields above 9 kOe were fitted using the Law of Approach to Saturation (LAS) for cubic anisotropy systems[7,23] given by

$$|M(H)| = M_s - \frac{8{K_1}^2}{105{\mu_0}^2 M_s H^2} + \kappa H, \tag{4}$$

where K_1 is the first order cubic magnetocrystalline anisotropy constant. The numerical coefficient $\frac{8}{105}$ has been obtained for a polycrystalline material. The last term κH represents forced magnetization due to the increase of saturation

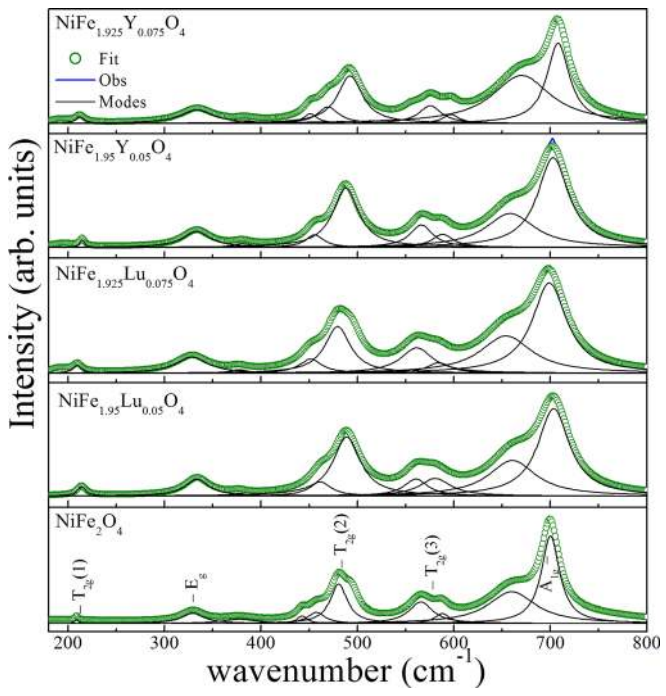

FIG. 5. Room temperature Raman spectra of $NiFe_{2-x}R_xO_4$ (R = Y and Lu; $x = 0$, 0.05, and 0.075).

TABLE II. Positions of $T_{2g}(3)$ Raman modes.

Compound	$T_{2g}(3)$ Peak 1 (cm^{-1})	$T_{2g}(3)$ Peak 2 (cm^{-1})
$NiFe_2O_4$	564.90	588.73
$NiFe_{1.95}Lu_{0.05}O_4$	560.63	580.7
$NiFe_{1.925}Lu_{0.075}O_4$	559.44	581.89
$NiFe_{1.95}Y_{0.05}O_4$	566.50	588.97
$NiFe_{1.925}Y_{0.075}O_4$	575.98	597.24

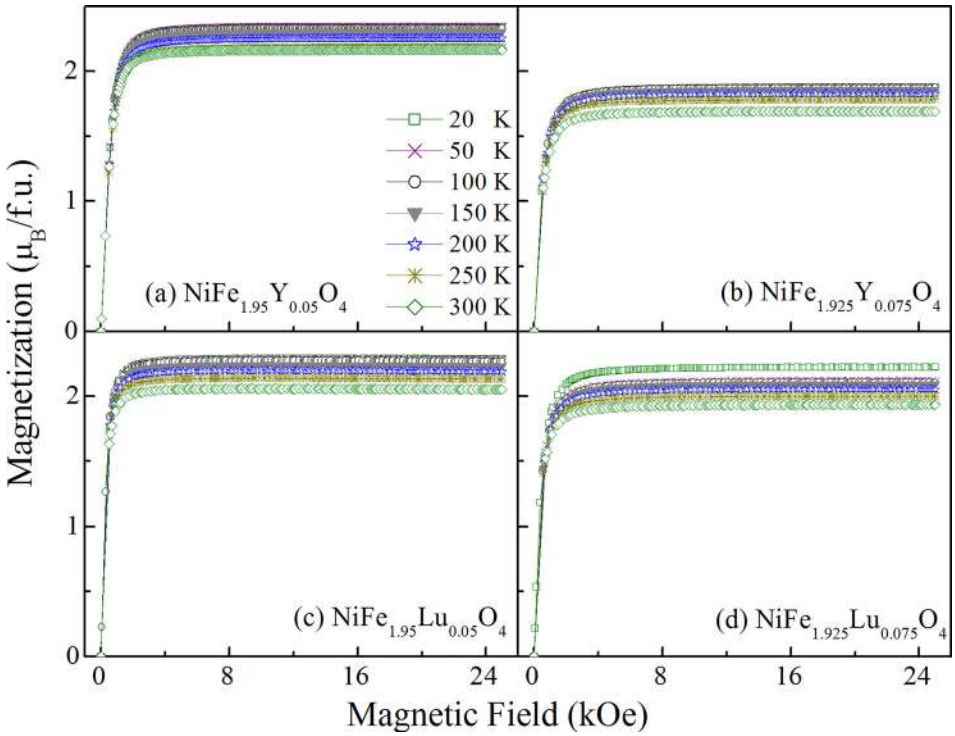

FIG. 6. Magnetization of $NiFe_{2-x}Y_xO_4$ ($x = 0.05$ (a) and 0.075 (b)) and $NiFe_{2-x}Lu_xO_4$ ($x = 0.05$ (c) and 0.075 (d)) recorded at 20 K, 50 K, 100 K, 150 K, 200 K, 250 K, and 300 K.

magnetization in high fields, where κ represents paramagnetic susceptibility, which was neglected in the present case as there are no paramagnetic impurities. Fig. 7 shows the values of K_1 of $NiFe_{2-x}R_xO_4$ (R = Y and Lu; $x = 0$, 0.05, and 0.075) in the temperature range of 20 K–300 K. The value of K_1 of $NiFe_2O_4$ is 4.2×10^4 J/m^3 at 20 K and is 3.3×10^4 J/m^3 at 300 K. The reported value of K_1 of the $NiFe_2O_4$ single crystal is 0.62×10^4 J/m^3 at 300 K (Refs. 36 and 37) and of $NiFe_2O_4$ nanoparticles is 3.48×10^4 J/m^3 at 5 K and 1.8×10^4 J/m^3 at 300 K.[4] In the present case, the slightly higher value of K_1 of $NiFe_2O_4$ is attributed to the large average particle sizes of the polycrystalline compounds, which is found to be in the range of 1 μm–2 μm.

The values of K_1 of $NiFe_{2-x}Y_xO_4$ at 20 K are 5.4×10^4 J/m^3 and 5.0×10^4 J/m^3 for $x = 0.05$ and 0.075, respectively, and of $NiFe_{2-x}Lu_xO_4$ at 20 K are 5.3×10^4 J/m^3 and 5.6×10^4 J/m^3 for $x = 0.05$ and 0.075, respectively. The substitution of Y^{3+}/Lu^{3+} for Fe^{3+} (ionic radii of Y^{3+}, Lu^{3+}, and Fe^{3+} are 0.89 Å, 0.85 Å, and 0.63 Å, respectively) resulted in the increased lattice constant and O^{2-}-Fe^{3+}(B) bond lengths and altered the Fe^{3+}(A)-O^{2-}-Fe^{3+}/R^{3+}(B) bond angles. This caused a small distortion of the lattice and a corresponding increase of anisotropy.

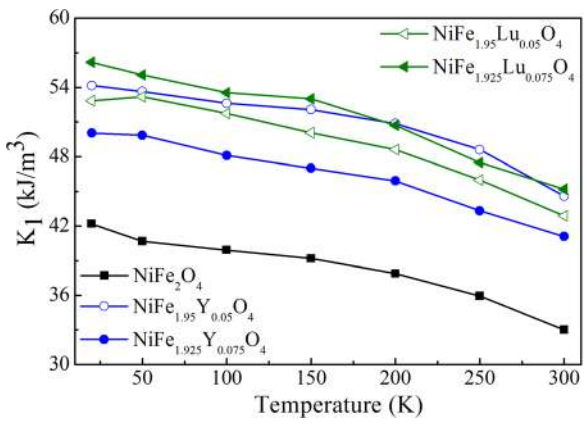

FIG. 7. The first order cubic magnetocrystalline anisotropy constant (K_1) *vs* temperature of $NiFe_{2-x}R_xO_4$ (R = Y and Lu; $x = 0$, 0.05 and 0.075).

Fig. 8 shows the indexed ND patterns along with the magnetic structure of $NiFe_{2-x}R_xO_4$ (R = Y and Lu; $x = 0$ and 0.075) at 300 K. The Rietveld refinement was carried out using the FULLPROF program. The Thompson-Cox-Hastings pseudo-Voigt function was employed for the fitting. All the peaks correspond to the cubic inverse spinel phase ($Fd\bar{3}m$). The magnetic moments of Fe^{3+} and Ni^{2+} along with the refinement parameters (both the crystal and magnetic) are given in Table III. As expected, decreased m_B and the net magnetic moment of $NiFe_{1.925}R_{0.075}O_4$ (R = Y and Lu) compared to those of $NiFe_2O_4$ are observed. The negative sign of $\vec{m}_B$ indicates the antiparallel alignment of $\vec{m}_B$ with $\vec{m}_A$.

E. Mössbauer studies

Figs. 9(a)–9(c) show the Mössbauer spectra of $NiFe_2O_4$ and $NiFe_{1.925}R_{0.075}O_4$ (R = Y, Lu) compounds, respectively, recorded at 5 K. The Mössbauer spectra were fitted with the NORMOS program. All spectra were fit to two sextets corresponding to the Fe^{3+} ions at the tetrahedral and octahedral sites. Table IV gives the hyperfine fields (H_{eff}), isomer shifts (IS), quadrupole shifts (QS), line widths (τ), and intensity ratios (I %) obtained from the fitting. The sextet with a larger hyperfine field is assigned to the Fe^{3+} ions at the B-site, whereas the sextet with smaller hyperfine field is assigned to the Fe^{3+} ions occupying the A-site.[38–40] Thus, in $NiFe_2O_4$, the hyperfine fields 51.0 T and 55.4 T are assigned to the A and B sites, respectively. These values are in good agreement with those reported for bulk $NiFe_2O_4$.[40–42] The hyperfine

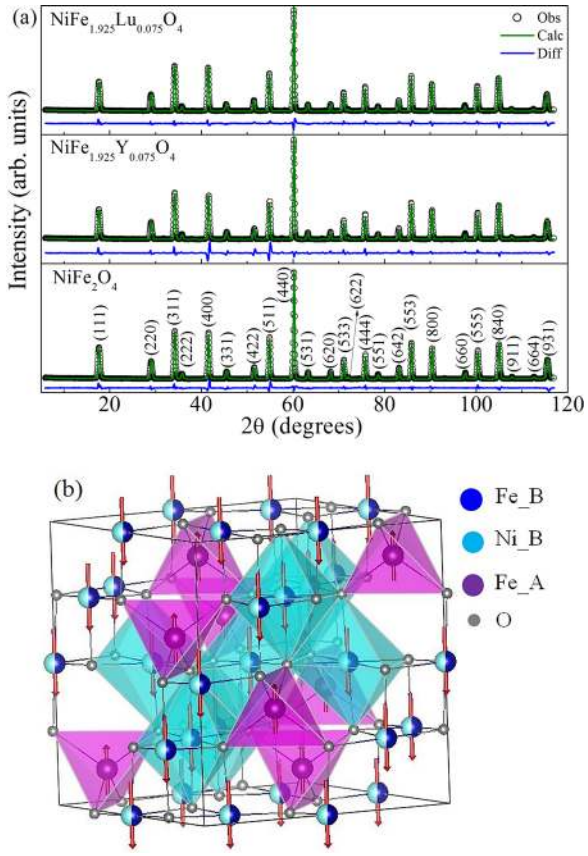

FIG. 8. ND pattern of $NiFe_{2-x}R_xO_4$ (R = Y and Lu; $x = 0$ and 0.075) at 300 K: Indexed Rietveld refined pattern (a) and magnetic structure of $NiFe_2O_4$ (b).

fields at the B-site in $NiFe_{1.925}R_{0.075}O_4$ (R = Y and Lu) compounds are seen to be the less than that in $NiFe_2O_4$, and this reduction is attributed to the substitution of non-magnetic Y^{3+} or Lu^{3+} ions for Fe^{3+}, causing reduction in the number of

TABLE III. Structural and magnetic parameters of $NiFe_{2-x}R_xO_4$ ($x = 0$ and 0.075; R = Y and Lu) from ND studies.

Compound		$NiFe_2O_4$	$NiFe_{1.925}Y_{0.075}O_4$	$NiFe_{1.925}Lu_{0.075}O_4$
a(Å)		8.3402(3)	8.3430(8)	8.34630(2)
Bragg-R factors	Bragg-R	5.29	4.64	3.24
	R_f-factor	3.20	3.43	2.54
	χ^2	1.45	2.91	1.18
	Mag-R	9.95	5.95	6.92
Reliability factors	R_p	5.37	7.09	5.23
	R_{wp}	7.87	11.1	7.03
	R_{exp}	6.54	6.52	6.48
A-site (μ_B/f.u.)	Fe^{3+}	2.64	2.67	2.55
B-site (μ_B/f.u.)	Fe^{3+}	−4.32	−4.04	−4.02
	Ni^{2+}	−1.22	−1.20	−1.21
	R^{3+}	…	0	0
Net moment A-site (μ_B/f.u.)		2.64	2.67	2.55
Net moment B-site (μ_B/f.u.)		−5.54	−5.24	−5.23
Net moment (μ_B/f.u.)		2.9	2.57	2.68

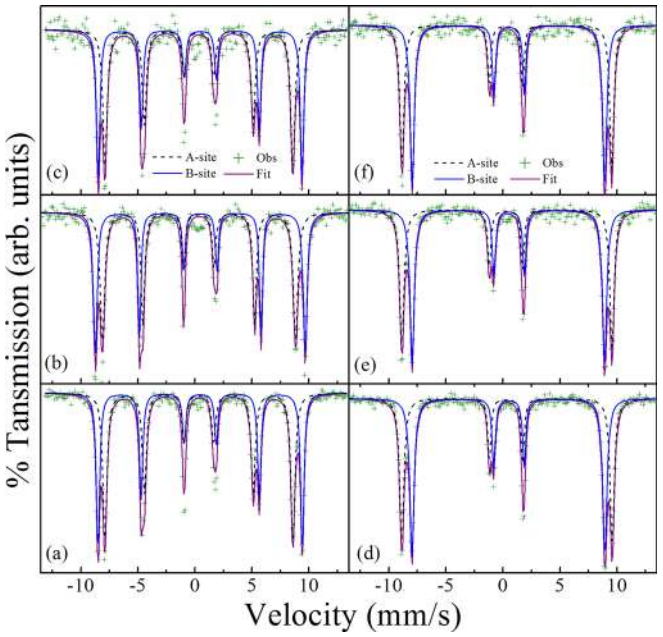

FIG. 9. Mössbauer spectra of $NiFe_2O_4$ ((a) and (d)), $NiFe_{1.925}Y_{0.075}O_4$ ((b) and (e)), and $NiFe_{1.925}Lu_{0.075}O_4$ ((c) and (f)) compounds recorded at 5 K. (d), (e), and (f) represents spectra recorded with a magnetic field of 5 T applied parallel to the γ-ray direction.

Fe^{3+} ions at the B-site. A decrease in hyperfine fields with partial substitution of Fe^{3+} by magnetic ions such as Cr^{3+},[41] Sm^{3+}, Gd^{3+}, and Dy^{3+} (Ref. 42) at the B-site in $NiFe_2O_4$ has been reported. Figs. 9(d), 9(e), and 9(f) show the Mössbauer spectra of $NiFe_2O_4$ and $NiFe_{1.925}R_{0.075}O_4$ (R = Y and Lu) compounds, respectively, recorded in a magnetic field of 5 T applied in the direction of propagation of γ-ray. The spectra revealed the absence of the 2nd and 5th lines, corresponding to the transitions $m_l = \pm\frac{1}{2}$ to $\pm\frac{1}{2}$ (i.e., $\Delta m_l = 0$),[43,44] respectively. The transitions of $m_l = \pm\frac{3}{2}$ to $\pm\frac{1}{2}$ (i.e., $\Delta m_l = \pm 1$) are represented by the highest intensity, and the transitions $m_l = \mp\frac{1}{2}$ to $\pm\frac{1}{2}$ (i.e., $\Delta m_l = \pm 1$) are represented by the lowest intensity.[43,44] For a random orientation of magnetic moments, the intensity ratio is 3:2:1, and when the spins are oriented in the direction of the field, the ratio is 3:0:1.[39,40,43] The intensity ratios in Figs. 9(d), 9(e), and 9(f) match with 3:0:1, indicating the orientation of moments in the direction of propagation of γ-ray. This confirms the collinear magnetic moments in all the compounds investigated.

Table V shows the hyperfine parameters obtained from the spectra recorded in the presence of the applied field. Under a magnetic field, large enough to saturate the moments, the magnetic moments and thus the hyperfine field at the A site are aligned parallel (increased H_{eff}) and those at the B site are aligned antiparallel (thus decreased H_{eff}) to the applied field.[38,39] The hyperfine fields of 57.1 T in $NiFe_2O_4$, 57.0 T and 56.9 T, respectively, in Y^{3+} and Lu^{3+} substituted $NiFe_2O_4$, are assigned to the Fe^{3+} ions at the A-site, whereas the hyperfine fields of 52.4 T in $NiFe_2O_4$, 52.2 T and 52.3 T, respectively, in Y^{3+} and Lu^{3+} substituted $NiFe_2O_4$, are assigned to those at the B-site. In $NiFe_2O_4$, under an external magnetic field, increased hyperfine fields at the A-site and decreased hyperfine fields at the B-site have been reported by Ahlawat *et al.*[40]

TABLE IV. Hyperfine parameter (at 5 K) values of $NiFe_{2-x}R_xO_4$ ($x = 0$ and 0.075; R = Y and Lu).

	$NiFe_2O_4$		$NiFe_{1.925}Y_{0.075}O_4$		$NiFe_{1.925}Lu_{0.075}O_4$	
Sample Site	A	B	A	B	A	B
T (mm/s)	0.425 ± 0.015	0.353 ± 0.007	0.427 ± 0.017	0.357 ± 0.009	0.436 ± 0.015	0.358 ± 0.019
IS (mm/s)	0.348 ± 0.004	0.458 ± 0.002	0.342 ± 0.004	0.457 ± 0.003	0.346 ± 0.005	0.461 ± 0.005
QS (mm/s)	0.013 ± 0.004	−0.006	0.022 ± 0.006	−0.010 ± 0.004	−0.015 ± 0.007	−0.019 ± 0.009
H_{eff} (T)	51.07 ± 0.01	55.47 ± 0.03	50.98 ± 0.03	55.40 ± 0.02	51.02 ± 0.05	55.33 ± 0.03
I %	53.38	46.62	52.31	47.68	53.49	46.51

TABLE V. Hyperfine parameter (in 5 T applied field at 5 K) values of $NiFe_{2-x}R_xO_4$ ($x = 0$ and 0.075; R = Y and Lu).

	$NiFe_2O_4$		$NiFe_{1.925}Y_{0.075}O_4$		$NiFe_{1.925}Lu_{0.075}O_4$	
Sample Site	A	B	A	B	A	B
T (mm/s)	0.331 ± 0.005	0.347 ± 0.005	0.340 ± 0.010	0.346 ± 0.008	0.326 ± 0.010	0.336 ± 0.011
IS (mm/s)	0.312 ± 0.002	0.501 ± 0.002	0.305 ± 0.003	0.505 ± 0.004	0.304 ± 0.007	0.509 ± 0.008
QS (mm/s)	0.083 ± 0.005	−0.047 ± 0.005	0.088 ± 0.008	0.062 ± 0.007	0.079 ± 0.009	0.053 ± 0.017
H_{eff} (T)	57.13 ± 0.01	52.41 ± 0.01	57.06 ± 0.02	52.29 ± 0.02	56.98 ± 0.04	52.29 ± 0.04
I %	47.30	52.70	47.15	52.85	46.47	53.53

The isomer shifts (IS) at the B-site are more than those at the A-site in all the compounds investigated. The Fe^{3+} (B-site)-O^{2-} bond lengths are higher than the Fe^{3+} (A-site)-O^{2-} bond lengths (see Table I), leading to higher values of the IS at the B-site.

The average canting angle (θ)[44] was calculated from the equation

$$\theta = \cos^{-1}\left[\sqrt{\frac{4 - I_2/I_3}{4 + I_2/I_3}}\right], \tag{5}$$

where I_2 and I_3 are intensities of the 2nd and 3rd lines, respectively, in a given sextet. From Figs. 9(d)–9(f), the absence of the second line ($I_2 = 0$) confirms that the canting angle is zero. The degree of inversion or inversion parameter (λ)[45] in the compounds was calculated as

$$\frac{I_A}{I_B} = \frac{f_A}{f_B}\frac{\lambda}{2 - \lambda}, \tag{6}$$

where I_A and I_B are the integrated intensity area percentage of the sextets, assigned to the A and B sites, respectively; f_A and f_B are recoilless fractions of the A and B sites, respectively. The ratio f_A/f_B has been reported to be 1 at 0 K and 0.94 at 300 K.[45] Using the relative intensities given in Table V along with Eq. (6), the calculated degrees of inversion are found to be 0.94 ± 0.02 in $NiFe_2O_4$, 0.94 ± 0.04 and 0.93 ± 0.04, respectively, in Y and Lu substituted $NiFe_2O_4$, which are in agreement with those obtained from the refinement of XRD patterns and magnetization. Thus, all the three compounds exhibit a near complete inverse spinel structure along with Néel-type collinear spin arrangement.

Using Eqs. (2) and (3) and the above inversion parameter values, the onsite and net magnetic moments were calculated. The Fe^{3+} B-site magnetic moments were obtained as 5.27 μ_B for $NiFe_2O_4$, 4.91 μ_B and 4.98 μ_B, respectively, for R = Y and Lu in $NiFe_{1.925}R_{0.075}O_4$. This decrease in the B-site magnetic moments confirms that Y^{3+} and Lu^{3+} occupy the B-site. On the other hand, the magnetic moments of the Fe^{3+} ions at the A-site are 4.72 μ_B for $NiFe_2O_4$, 4.71 μ_B and 4.64 μ_B, respectively, for R = Y and Lu in $NiFe_{1.925}R_{0.075}O_4$, attributed to different values of inversion parameters of the respective compounds. The net magnetic moments determined from the Mössbauer spectra in the presence of the magnetic field are found to be 2.60 μ_B/f.u. for $NiFe_2O_4$, 2.33 μ_B/f.u. and 2.30 μ_B/f.u., respectively, for R = Y and Lu in $NiFe_{1.925}R_{0.075}O_4$. Thus, (partial) substitution of non-magnetic Y^{3+} and Lu^{3+} ions for Fe^{3+} results in a decrease in the onsite and net magnetic moment values. However, the moment values obtained from Mössbauer spectra (recorded at 5 T) are slightly higher than calculated (using the Hund's rules) and measured through magnetization. This can be attributed to different values of inversion parameters (obtained from Equation (6)) of the respective compounds.

IV. CONCLUSIONS

$NiFe_{2-x}R_xO_4$ (R = Y and Lu; $x = 0$, 0.05, and 0.075) compounds crystallize in the cubic inverse spinel phase as confirmed by XRD and Raman spectroscopy. An increase in the O-B bond length and lattice constant and a decrease in the O-A bond length and *u*-parameter were observed. In addition, the decrease in Fe^{3+} B-site occupancies confirms the occupation of Y^{3+} or Lu^{3+} ions at the B-site. The oxidation states of cations were found to be +3 for Fe (92%) and Y and +2 for Ni from the XPS measurements. The degrees of inversion values obtained from refined XRD patterns, magnetization, and Mössbauer studies are seen to match. Neutron diffraction and Mössbauer studies revealed a collinear ferrimagnetic structure and a nearly perfect inverse spinel structure. The B-site magnetic moment (and hence net

magnetic moment) was found to decrease with the Y^{3+} or Lu^{3+} content.

ACKNOWLEDGMENTS

The authors thank the Indian Institute of Technology (IIT) Madras, India, for providing the DST-FIST (Department of Science and Technology - Fund for Improvement of Science and Technology) facility for SQUID measurements and UGC-DAE Consortium for Scientific Research: (a) Mumbai Center, Bhabha Atomic Research Centre, Trombay, Mumbai-400 085, India, for ND measurements. (b) Indore Center, Madhya Pradesh - 452 001, India, for Mössbauer measurements. K. Ugendar thanks IIT Madras for the financial support.

[1]S. Matzen, J. B. Moussy, P. Wei, C. Gatel, J. C. Cezar, M. A. Arrio, P. Sainctavit, and J. S. Moodera, Appl. Phys. Lett. **104**, 182404 (2014).
[2]N. M. Caffrey, D. Fritsch, T. Archer, S. Sanvito, and C. Ederer, Phys. Rev. B **87**, 024419 (2013).
[3]U. Luders, A. Barthelemy, M. Bibes, K. Bouzehouane, S. Fusil, E. Jacquet, J. P. Contour, J. F. Bobo, J. Fontcubera, and A. Fert, Adv. Mater. **18**, 1733 (2006).
[4]B. K. Chatterjee, C. K. Ghosh, and K. K. Chattopadhyay, J. Appl. Phys. **116**, 153904 (2014).
[5]V. K. Verma, V. R. Singh, K. Ishigami, G. Shibata, T. Harano, T. Kadono, A. Fujimori, F.-H. Chang, H.-J. Lin, D.-J. Huang, C. T. Chen, Y. Zhang, J. Liu, Y. Lin, C.-W. Nan, and A. Tanaka, Phys. Rev. B **89**, 115128 (2014).
[6]J. Smith and H. P. J. Wijin, *Ferrites* (Philips Technical Library, Eindhoven, The Netherlands, 1965).
[7]S. Chikazumi, *Physics of Ferromagnetism* (Oxford University Press, New York, 1997).
[8]S. Panchal, S. Raghuvanshi, K. Gehlot, F. Mazaleyrat, and S. N. Kane, AIP Adv. **6**, 055930 (2016).
[9]C. M. B. Henderson, J. M. Charnock, and D. A. Plant, J. Phys.: Condens. Matter **19**, 076214 (2007).
[10]S. N. Piramanayagam, J. Appl. Phys. **102**, 011301 (2007).
[11]J.-U. Thiele, S. Maat, and E. E. Fullerton, Appl. Phys. Lett. **82**, 2859 (2003).
[12]J. Chappert and R. B. Frankel, Phys. Rev. Lett. **19**, 570 (1967).
[13]Z. K. Heiba, M. B. Mohamed, M. Ahmed, M. Moussa, and H. Hamdehe, J. Alloys Compd. **586**, 773 (2014).
[14]A. Ghasemin and M. Mousavinia, Ceram. Int. **40**, 2825 (2014).
[15]M. Şoka, M. Uşáková, R. Dosoudil, E. Uşák, and E. Dobroçka, IEEE Trans. Magn. **51**, 2000504 (2015).
[16]K. K. Bharathi, J. A. Chelvane, and G. Markandeyulu, J. Magn. Magn. Mater. **321**, 3677 (2009).
[17]C. Murugesan and G. Chandrasekaran, RSC Adv. **5**, 73714 (2015).
[18]M. Şoka, M. Uşáková, E. Uşák, R. Dosoudil, and J. Lokaj, IEEE Trans. Magn. **50**, 2800304 (2014).
[19]N. Rezlescu, E. Rezlescu, C. Pasnicu, and M. L. Craus, J. Phys.: Condens. Matter **6**, 5707 (1994).
[20]R. R. Kiran, R. A. Mondal, S. Dwevedi, and G. Markandeyulu, J. Alloys Compd. **610**, 517–521 (2014).
[21]K. K. Bharathi, G. Markandyulu, and C. Ramana, J. Phys. Chem. C **115**, 554 (2011).
[22]K. K. Bharathi, K. Balamurugan, P. N. Santhosh, M. Pattabiraman, and G. Markandyulu, Phys. Rev. B **77**, 172401 (2008).
[23]K. Ugendar, V. R. Reddy, and G. Markandeyulu, IEEE Trans. Magn. **52**, 2500106 (2016).
[24]H. S. Aziz, S. Rasheed, R. A. Khan, A. Rahim, J. Nisar, S. M. Shah, F. Iqbal, and A. R. Khan, RSC Adv. **6**, 6589 (2016).
[25]M. Yehia, S. Ismail, and A. Hashhash, J. Supercond. Nov. Magn. **27**, 771–774 (2014).
[26]J. M. R. Gonzblez and C. O. Areh, J. Chem. Soc. Dalton Trans. **1985**, 2155 (1985).
[27]M. Amer and M. E. Hiti, J. Magn. Magn. Mater. **234**, 118 (2001).
[28]K. J. Kim, M. H. Kim, and C. S. Kim, J. Magn. **19**, 111 (2014).
[29]J. J. Chambers and G. N. Parsons, Appl. Phys. Lett. **77**, 2385 (2000).
[30]S. Mondal, C.-H. Chueh, and T.-M. Pan, J. Appl. Phys. **115**, 014501 (2014).
[31]P. Graves, C. Johnston, and J. Campaniello, Mater. Res. Bull. **23**, 1651 (1988).
[32]V. G. Ivanov, M. Abrashev, M. Iliev, M. M. Gospodinov, J. Meen, and M. Aroyo, Phys. Rev. B **82**, 024101 (2010).
[33]M. N. Iliev, D. Mazumdar, J. X. Ma, A. Gupta, F. Rigato, and J. Fontcuberta, Phys. Rev. B **83**, 014108 (2011).
[34]Z. X. Cheng, H. Shen, J. Y. Xu, P. Liu, S. J. Zhang, J. L. Wang, X. L. Wang, and S. X. Dou, J. Appl. Phys. **111**, 034103 (2012).
[35]W. Zhu, L. Pi, S. Tan, and Y. Zhang, Appl. Phys. Lett. **100**, 052407 (2012).
[36]B. D. Cullity, in *Introduction to Magnetic Materials*, edited by M. Cohen (Addison-Wesley Publishing Company, Inc. Philippines, 1972).
[37]W. A. Yager, J. K. Galt, and F. R. Merritt, Phys. Rev. **99**, 1203 (1955).
[38]G. A. Sawatzky, F. V. D. Woude, and A. H. Morrish, Phys. Lett. A **25**, 147 (1967).
[39]C. N. Chinnasamy, A. Narayanasamy, N. ponpandian, K. Chattopadhyay, K. Shinoda, K. T. B. Jeyadevan, K. Nakatsuka, T. Furubayashi, and I. Nakatani, Phys. Rev. B **63**, 184108 (2001).
[40]A. Ahlawat, V. G. Sathe, V. R. Reddy, and A. Gupta, J. Magn. Magn. Mater. **323**, 2049 (2011).
[41]A. M. Gismelseed and A. A. Yousif, Physica B **370**, 215 (2005).
[42]S. S. R. Inbanathan, V. Vaithyanathan, J. A. Chelvane, G. Markandeyulu, and K. K. Bharathi, J. Magn. Magn. Mater. **353**, 41 (2014).
[43]V. G. Bhide, *Mössbauer Effect and Its Applications* (Tata McGraw-Hill Publishing Company, 1973).
[44]G. A. Petitt and D. W. Forester, Phys. Rev. B **4**, 3912 (1971).
[45]G. A. Sawatzky, F. V. D. Woude, and A. H. Morrish, Phys. Rev. B **183**, 383 (1969).